Bone marrow graft-versus-host disease: early destruction of hematopoietic niche after MHC-mismatched hematopoietic stem cell transplantation

Yusuke Shono,[1,2] Satoshi Ueha,[1] Yong Wang,[1] Jun Abe,[1] Makoto Kurachi,[1] Yoshihiro Matsuno,[3] Tatsuki Sugiyama,[4] Takashi Nagasawa,[4] Masahiro Imamura,[2] and Kouji Matsushima[1]

[1]Department of Molecular Preventive Medicine, Graduate School of Medicine, The University of Tokyo, Tokyo; [2]Department of Hematology and Oncology, Hokkaido University Graduate School of Medicine, Sapporo; [3]Department of Surgical Pathology, Hokkaido University Hospital, Sapporo; and [4]Department of Immunobiology and Hematology, Institute for Frontier Medical Sciences, Kyoto University, Kyoto, Japan

Disrupted hematopoiesis and delayed immune reconstitution are life-threatening complications of allogeneic hematopoietic stem cell transplantation (allo-HSCT). Although graft-versus-host disease (GVHD) is a major risk factor for the bone marrow (BM) insufficiency, how GVHD impairs BM hematopoiesis has been largely unknown. We hypothesized that BM stromal niche could be a target of GVHD. In major histocompatibility complex (MHC)–mismatched murine models of GVHD, we have demonstrated the early destruction of osteoblasts that especially affected B-cell lineages. The defective B lymphopoiesis was due to the impaired ability of BM stroma and osteoblasts to support the hematopoiesis, as evidenced by the failure of GVHD-affected BM to reconstitute the hematopoietic cells. The administration of anti-CD4 monoclonal antibody (mAb) ameliorated these effects and improved B lymphopoiesis while preserving graft-versus-tumor effects. Genetic ablation of Fas–Fas ligand signaling also partially restored B lymphopoiesis. Our present study provided evidence of BM GVHD, with the identification of osteoblasts as the main target for GVHD in BM. Moreover, our data showed the potential for mAb therapies to enhance immune reconstitution in vivo for patients undergoing allo-HSCT. (*Blood*. 2010;115(26): 5401-5411)

Introduction

Graft-versus-host disease (GVHD) is a major complication after allogeneic hematopoietic stem cell transplantation (allo-HSCT). The principal organs affected by GVHD are the skin, liver, gastrointestinal tract, and lung.[1,2] However, bone marrow (BM) suppression without infection is often observed in patients undergoing allo-HSCT as GVHD symptoms appear, suggesting that BM could be a target of GVHD. Complications considered to result from BM dysfunction, such as infections after delayed immune reconstitution or bleeding, account for approximately 30% of deaths after allo-HSCT.[3] Although BM is a likely target for GVHD and its dysfunction could have a serious negative impact on clinical outcomes, the mechanism for the BM dysfunction associated with GVHD is still unclear.

Clinical and experimental data have shown that immunologic reconstitution is impaired by GVHD,[4-7] and GVHD-associated myelosuppression and lymphoid hypoplasia have been reported.[8-10] One important finding is the possible involvement of Fas ligand signal provided by donor T cells in the impairment of B lymphopoiesis during GVHD.[9] It has however remained elusive how Fas signaling provided by donor T cells impairs B lymphopoiesis of donor hematopoietic stem cell (HSC) origin.

In the BM, hematopoiesis is dependent on specialized microenvironments, known as hematopoietic niches, to maintain blood cells.[11] Osteoblasts on bone surfaces[12-14] and endothelial cells[15] lining sinusoids establish hematopoietic niches in the BM. Moreover, chemokine (C-X-C motif) ligand 12 (CXCL12)–abundant reticular (CAR) cells, surrounding sinusoidal endothelial cells or located near the endosteum, are thought to be involved in hematopoiesis, including HSC maintenance and B-cell development.[16-19]

To date, little research has been done to clarify the mechanism of BM dysfunction during GVHD, especially with respect to the role of hematopoietic niches. In this study, we evaluated the effect of GVHD on BM, especially on its hematopoietic niches, using models of allo-HSCT in major histocompatibility complex (MHC)–mismatched, lethally irradiated mice.

Methods

Mice and cell lines

Female C57BL/6 (B6; $K^bD^bI\text{-}A^bI\text{-}E^b$, CD45.2$^+$) and (C57BL/6 × DBA/2) F_1 (BDF_1; H-$2^{b\times d}$, CD45.2$^+$) mice were purchased from CLEA Japan, Inc. C57BL/6.SJL (B6.SJL; *Ptprc^a Pepc^b*, CD45.1$^+$), B6.C-$H2^{bm1}$(bm1; $K^{bm1}D^bI\text{-}A^bI\text{-}E^b$, CD45.2$^+$), and B6.C-$H2^{bm12}$(bm12; $K^bD^bI\text{-}A^{bm12}I\text{-}E^b$, CD45.2$^+$) mice were purchased from The Jackson Laboratory. bm1 and bm12 mice possess mutant MHC class I and class II alleles, respectively. Fas-defective B6.*lpr* ($B6^{lpr/lpr}$; H-2^b, CD45.2$^+$) and Fas ligand–defective B6.*gld* ($B6^{gld/gld}$; H-2^b, CD45.2$^+$) were obtained from SLC Japan, Inc. CXCL12–green fluorescent protein (GFP) knock-in mice[20] were backcrossed more than 7 times with B6 (CD45.2$^+$) mice, and then, crossed with DBA/2 mice to make CXCL12-GFP knock-in mice (BDF_1). Mice used for experiments were 6 to 8 weeks old at the time of allo-HSCT. Mice were maintained in a specific pathogen–free condition, and all animal experimentation was conducted in accordance with institutional guidelines with the approval of

Submitted November 10, 2009; accepted March 22, 2010. Prepublished online as *Blood* First Edition paper, March 30, 2010; DOI 10.1182/blood-2009-11-253559.

An Inside *Blood* analysis of this article appears at the front of this issue.

The online version of this article contains a data supplement.

The publication costs of this article were defrayed in part by page charge payment. Therefore, and solely to indicate this fact, this article is hereby marked "advertisement" in accordance with 18 USC section 1734.

Table 1. Transplantation models

	MHC haplotype			Donor cells		
				TCD BM	T cells	
Experimental models	Recipient	Donor	MHC disparity	Genotype	Subsets	Genotype
[B6→BDF$_1$] (BM/T)						
WT/−	H-2$^{b/d}$	H-2^{b}	MHC I and II	WT	—	—
WT/WT	H-2$^{b/d}$	H-2^{b}	MHC I and II	WT	CD4/CD8	WT
lpr/−	H-2$^{b/d}$	H-2^{b}	MHC I and II	Fas$^{lpr/lpr}$	—	—
lpr/WT	H-2$^{b/d}$	H-2^{b}	MHC I and II	Fas$^{lpr/lpr}$	CD4/CD8	WT
WT/gld	H-2$^{b/d}$	H-2^{b}	MHC I and II	WT	CD4/CD8	FasL$^{gld/gld}$
[B6→bm$_1$]	H-2^{bm1}	H-2^{b}	MHC I	WT	CD8	WT
[B6→bm$_{12}$]	H-2^{bm12}	H-2^{b}	MHC II	WT	CD4	WT
[B6$^{gld/gld}$→bm$_{12}$]	H-2^{bm12}	H-2^{b}	MHC II	WT	CD4	FasL$^{gld/gld}$

Congenic markers of each donor-recipient pair is otherwise indicated. *lpr* and *gld* are loss-of-function mutation of Fas and FasL, respectively. Groups are labeled as source of BM/source of splenic T cells (BM/T).

the animal care and use committee of the University of Tokyo. P815 (H-2^{d}) cell lines were originally provided from Dr Abe (Nipponkayaku).

HSCT and tumor induction

BM cells were prepared from the femurs and tibiae of B6 donor mice and depleted of Thy1.2^{+} mature T cells using the autoMACS system (Miltenyi Biotec). Splenic cells were prepared from donor mice. T cells, CD4^{+} cells, and CD8^{+} T cells were negatively enriched by autoMACS with antibody against CD11b, B220, Ter-119, and NK1.1 with or without CD8 or CD4 (the purity of T cells: CD3^{+}, $>$ 92%; CD4^{+} and CD8^{+}, $>$ 95%). Recipient mice were lethally irradiated with 11 Gy for BDF$_1$ and 8.5 Gy for B6, bm1, and bm12 mice on day −1 (split into 2 doses given 3 hours apart to reduce gastrointestinal toxicity). Lethally irradiated recipient mice were intravenously injected with 5×10^6 BM cells with or without 5×10^6 T cells. In experiments of graded CD4^{+} or CD8^{+} T-cell transfer, purified (contamination of CD4^{+} T cells in purified CD8^{+} T cells was $<$ 0.1%, and vice versa), graded numbers (2×10^5 to 2×10^7) of B6-derived CD4^{+} T cells or CD8^{+} T cells were separately transferred with T cell–depleted (TCD) BM cells into bm1/bm12 or BDF$_1$ recipient mice. Transplantation models including MHC mismatch and Fas–Fas ligand (FasL) defect are summarized in Tables 1 and 2. In graft-versus-tumor (GVT) experiments, recipients were intravenously injected with 1×10^4 P815 tumor cells 2 hours before transplantation. To evaluate the effects of GVHD on hematopoietic cells, lethally irradiated BDF$_1$ mice were received a transplant of 5×10^6 TCD BM from either bone marrow transplant (BMT) or GVHD recipient mice (donor mice were killed on day 14; Figure 4A). To evaluate the effects of GVHD on the potential of BM stroma to support hematopoiesis, BMT recipient mice or GVHD recipient mice were given 2 Gy total body irradiation (TBI) on day 13 after the first transplantation and received a second transplant of 5×10^6 TCD BM from normal C57BL/6.SJL donors the next day (Figure 4B). The recipient mice were killed on day 14 after the second transplantation and donor-derived hematopoiesis was analyzed. In the long-term competitive repopulation analysis (Figure 4C), CD45.2^{+} BDF$_1$ recipient mice received a transplant of CD45.1^{+} TCD BM with or without CD45.2^{+} T cells from B6 mice. BM CD45.2$^{−}$ cells were harvested from these recipient mice on day 14 after transplantation and were mixed with TCD BM from CD45.2^{+} untreated B6 mice at a ratio of 1:1. The cell mixtures were transferred into lethally irradiated B6 mice (CD45.2^{+}).

Table 2. Effects of Fas-FasL signaling blockage on B lymphopoiesis

Experimental models	Fas/FasL signaling		B lymphopoiesis
	Stroma	Blood cells	
[B6→BDF$_1$] (BM/T)			
WT/gld	×	×	○
lpr/WT	○	×	×
[B6$^{gld/gld}$→bm$_{12}$]	×	×	○

Groups are labeled as source of BM/source of splenic T cells (BM/T).

Systemic assessment of GVHD

The severity of GVHD was assessed with a clinical GVHD scoring system, as first described by Cooke et al.[21] Recipients were individually scored 2 or 3 times a week for 5 clinical parameters on a scale from 0 to 2: weight loss, posture, activity, fur texture, and skin integrity. A clinical GVHD index was generated by summation of the 5 criteria scores (0-10). Survival was monitored daily.

Histopathologic analysis, immunofluorescence staining, and histomorphometric analysis

For the histocytochemical analysis, femurs were fixed in 4% paraformaldehyde/phosphate-buffered saline (PBS) and embedded in paraffin after 5 days of decalcification in ethylenediaminetetraacetic acid solution (0.5 M). Tissue sections (5 μm) were stained with hematoxylin and eosin. Azan staining and silver impregnation were performed when evaluating elastic (collagenous) fibers. For the immunohistologic analysis and alkaline phosphatase (ALP) detection, fresh femoral bone samples were embedded in SCEM mounding medium (Leica Microsystems) and frozen in liquid nitrogen, and 5-μm cryosections were generated via the Kawamoto film method (Cryofilm transfer kit; Leica Microsystems). Immunofluorescent staining of fresh-frozen sections of intestinal tracts were performed as described previously.[22] In brief, cryosections were fixed with 4% paraformaldehyde/PBS and were preincubated with Block Ace (Dainippon Pharmaceutical Co Ltd). Subsequently, samples were incubated with primary antibodies against mouse immunoglobulin A (IgA; BD Biosciences), osteocalcin (Takara), MHC class II (M5/114.15.2; BD Biosciences), panendothelial cell antigen (MECA32; BioLegend), type IV collagen (Nihon Millipore K.K.), or appropriate control antibodies, followed by incubation with Alexa dye–labeled appropriate secondary reagents (Invitrogen Japan K.K.). The sections were analyzed by an Olympus IX-70 confocal laser-scanning microscope system (Olympus Optical Co Ltd). Staining for ALP activity was performed using Histofine Simple Stain Alkaline Phosphatase (Nichirei) according to manufacturer's protocol. Histologic analysis of CXCL12-GFP knock-in mice BM was performed as described previously.[18] In brief, bone samples were fixed in 4% paraformaldehyde and equilibrated in 30% sucrose/PBS. Fixed samples were embedded in OCT medium (Sakura) and frozen in cooled hexane. Sections of undecalcified femoral bone were generated via the Kawamoto film method. The sections were mounted with PERMAFLUOR (Beckman Coulter), and confocal microscopy was performed with a LSM 510 META (Carl Zeiss). Terminal deoxynucleotidyl transferase–mediated deoxyuridine triphosphate nick-end labeling assay was performed with In Situ Cell Death Detection Kit, TMR red (Roche Applied Sciences) according to manufacturer's protocol. Calcein double labeling of tibiae in recipient mice was performed with intraperitoneal injection of calcein (16 mg/kg body weight; Wako Pure Chemical Industries) on days 10 and 13 after transplantation. On day 14, left tibiae were removed and fixed in 70% ethanol and embedded in glycol-methacrylate without decalcification. The serial sections (5 μm in thickness) were cut longitudinally in the proximal region of the tibia and

stained with toluidine blue. Histomorphometry was performed with semiautomatic image analyzing system (HistometryRT; System-Supply). Histomorphometric measurements were made at ×400 using a minimum of 27 to 37 optical fields in the secondary spongiosa area from the growth plate–metaphyseal junction. Dynamic parameters were determined as follows. Single-labeled and double-labeled surfaces as well as total bone surface (BS) in the secondary spongiosa were traced at ×400 magnification. Then, single-labeled surface (sLS/BS, %) and double-labeled surface (dLS/BS, %) were calculated as a percentage of the total bone surface. Labeling width was determined as the average distance between the double labels. Mineral apposition rate (MAR, μm/day) was calculated by dividing the labeling width by the number of days between the 2 calcein administrations. Bone formation rate per bone surface (BFR/BS, $\mu m^3/\mu m^2$ per year) was the product of (sLS/2 + dLS) × MAR/BS. The nomenclature, symbols, and units used in this study are those recommended by the American Society for Bone Mineral Research Nomenclature Committee.

Flow cytometric analysis, platelet and red blood cell count, and cell sorting

Purified and fluorescein isothiocyanate (FITC)–, phycoerythrin (PE)–, allophycocyanin (APC)–, peridinin chlorophyll–cyanin 5.5 (Cy5.5)–, PE-Cy7–, APC-Cy7–, APC-Alexa750–, or biotin-conjugated anti–mouse monoclonal antibodies (mAbs) to FcγR (2.4G2), CD4 (RM4-5), CD5 (53-7.3), CD8α (53-6.7), CD11b (M1/70), CD19 (6D5), CD34 (RAM34), CD41 (MWReg30), CD44 (IM7), CD45R (RA3-6B2), CD45.1 (A20), CD45.2, (104) CD48 (HM48-1), CD61 (2C9.G2 [HMβ3-1]), CD62L (MEL-14), CD71 (RI7217), CD117 (c-Kit; 2B8), CD127 (interleukin-7 receptor [IL-7R]; A7R34), CD135 (Flt-3; A2F10), CD150 (9D1), Ly6A/E (Sca-1; E13-161.7), NK1.1 (PK136), Ter119 (TER-119), Ly-6G/C (Gr-1; RB6-8C5), and IgM (II/41), as well as isotype-matched control antibody and fluorescent dye–conjugated streptavidin were purchased from BD Biosciences, eBioscience, or BioLegend. After incubation with or without anti–mouse FcγRII/III mAb, cells were stained with appropriate concentrations of mAbs. Data were collected with EPICS ALTRA cell sorter (Beckman Coulter) or LSR-II flow cytometer (Becton Dickinson) and were analyzed with EXPO32 or FlowJo software (Version 8.5.2; TreeStar). Dead cells were excluded based on forward and side scatter profiles and propidium iodide or 4′,6-diamidino-2-phenylindole staining. Absolute number of platelets and red blood cells was determined using Celltac (Nihon Kohden) or flow cytometry using Flow-count (Beckman Coulter). For reverse transcription–polymerase chain reaction (RT-PCR) analysis, $c\text{-}Kit^+Lin^-$ cells were sorted using the EPICS ALTRA. The purity of sorted cells was routinely more than 98%.

ELISA and cytokine assay

Quantitative enzyme-linked immunosorbent assay (ELISA) immunoassay for fecal IgA was performed as described previously.[23] For analysis of serum immunoglobulins, blood serum was tested for IgA, IgM, and IgG using mouse ELISA Quantitation kit (Bethyl Laboratories). For cytokine assay in BM, the BM cells flushed from femurs and tibiae were suspended in RPMI-1640, containing 10% fetal bovine serum and 25 mM *N*-2-hydroxyethylpiperazine-*N*′-2-ethanesulfonic acid. Cytokine assay was performed using Bio-Plex Cytokine Assay Kit (Bio-Rad Laboratories) according to the manufacturer's instructions.

Real-time RT-PCR analysis

For quantitative real-time reverse-transcription polymerase chain reaction (RT-PCR), total RNA was isolated from sorted cells, whole BM cells, or whole tibia using TRIzol solution (Invitrogen Life Technologies) and reverse-transcribed with High Capacity cDNA Reverse Transcription Kit (Applied Biosystems). Whole tibia of each mouse was crushed using cryo-tissue-crasher (SK-200; Tokken Inc) before total RNA extraction. Real-time PCR was performed on Applied Biosystems PRISM 7500 sequence detection system using TaqMan probes or SYBR green incorporation with TaqMan Universal PCR Master Mix or Power SYBR Green PCR Master Mix (both from Applied Biosystems). The primers used for the PCR reaction are shown in supplemental Table 1 (available on the *Blood* Web site; see the Supplemental Materials link at the top of the online article). Values for each gene were normalized to the relative quantity of glyceraldehyde-3-phosphate dehydrogenase mRNA in each sample.

Evans blue extravasation assay

One percent Evans blue (EB: 0.2 mL/20-g mice) dissolved in sterile normal saline (0.9% NaCl) was injected via the tail vain. After 30 minutes, mice were killed and perfused with PBS through the left ventricle to clear the dye from the vascular volume. BM samples were frozen and crushed before EB extraction using formamide at 55°C for 16 hours. The optical density of the supernatant was determined spectrophotometrically at an excitation of 620 nm and an emission of 680 nm. The concentration of EB was determined from a standard curve.

In vivo T-cell subset depletion with monoclonal antibodies

For in vivo treatment, purified rat IgG2b anti–mouse CD4 mAb (GK1.5) and CD8 mAb (53-6.7) were purchased from BioXCell. Intraperitoneal administration of 200 μg of anti-CD4 and anti-CD8 mAb sufficiently depleted $CD4^+$ T cells and $CD8^+$ T cells, respectively, for at least 1 week after treatment (data not shown). Recipients were treated intraperitoneally with a dose of 200 μg on days 4 and 6 after allo-HSCT. Purified rat IgG was obtained from Jackson ImmunoResearch Laboratories Inc and injected intraperitoneally with the same dose as control recipients.

Statistical analysis

Survival curves were plotted using Kaplan-Meier estimates. The Mann-Whitney *U* test was used for the statistical analysis of in vitro data and clinical scores, whereas the Mantel-Cox log-rank test was used to analyze survival data (GraphPad Prism 5.00; GraphPad Software). A *P* value less than .05 was considered statistically significant.

Results

Hematopoietic profiles after allo-HSCT

We evaluated the effects of GVHD on hematopoiesis in (C57BL/6 × DBA/2) F_1 hybrid (BDF_1) mice transfused with fully MHC-mismatched, T cell–depleted (TCD) BM with splenic T cells from C57BL/6 (B6) donors after total body irradiation (TBI) with 11 Gy. Control BM transplant (BMT) mice received TCD BM alone after TBI. All mice in the GVHD group developed GVHD symptoms and died within 35 days after allo-HSCT (data not shown). The total numbers of BM, spleen, and thymic cells decreased during GVHD (Figure 1A). Kinetics of mature T and B cells, neutrophils, and monocytes in the BM and spleen indicated the suppression of hematopoiesis in the BM during GVHD (Figure 1B). We also examined the effects of GVHD on immature hematopoietic cells using a published classification.[24,25] The numbers of myeloid and lymphoid progenitors in BM decreased (Figure 1C). Strong expression of stem cell antigen 1 (Sca-1) resulted in a skewed profile of $c\text{-}Kit^+Sca\text{-}1^+Lin^-$ (KSL) cells (supplemental Figure 1A), leading to an increase in the number of KSL cells during GVHD, however $CD48^-CD150^+$KSL HSCs were also suppressed (Figure 1C and supplemental Figure 1A). We assessed erythroblast maturation as described previously[26] and found that erythropoiesis was also suppressed in the BM during GVHD (Figure 1D and supplemental Figure 1B). The absolute numbers of platelets and red blood cells decreased during GVHD (supplemental Figure 1C). Collectively, these data showed broad BM suppression in GVHD.

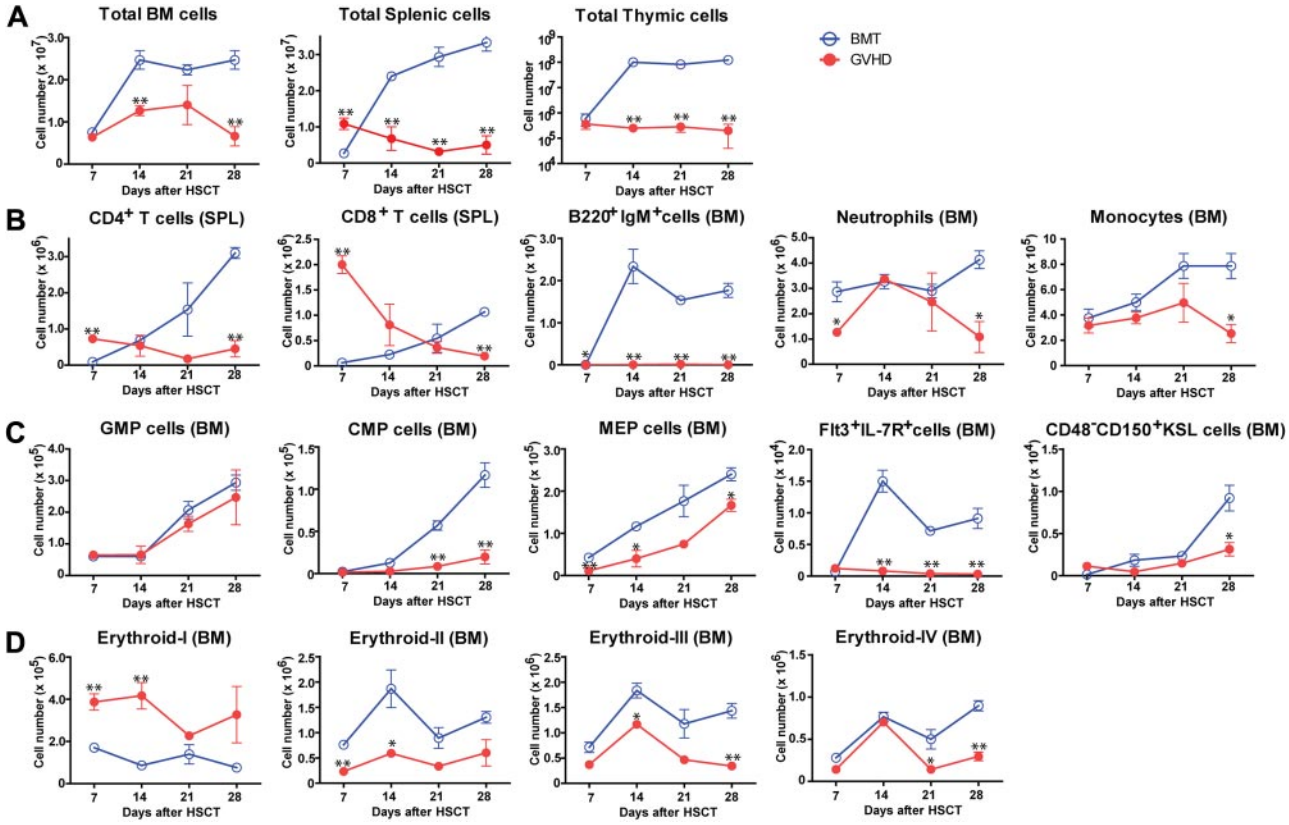

Figure 1. Suppression of hematopoiesis during GVHD. Lethally irradiated BDF_1 mice were implanted with B6 TCD BM alone (BMT) or with additional splenic T cells (GVHD). Cell populations were assessed weekly from days 7 to 28 after allo-HSCT. (A) Total cells in BM, spleen, and thymus. (B) Mature lymphoid and myeloid cells in spleen (SPL) and BM. (C) Myeloid and lymphoid progenitor cells and hematopoietic stem cells. GMP indicates granulocyte/macrophage lineage-restricted progenitor; CMP, common myeloid progenitor; MEP, megakaryocyte/erythrocyte lineage–restricted progenitor; and KSL, c-$Kit^+Sca\text{-}1^+Lin^-$. (D) Mature and immature erythropoietic cells. Data are mean ± SE from 1 of 2 to 4 experiments with similar results (n = 3 per group). $^*P < .05$; $^{**}P < .01$.

Suppression of B lymphopoiesis during GVHD

The hematopoietic profiles showed the kinetics of BM suppression during GVHD after allo-HSCT, consistent with clinical observations. As lymphopenia after allo-HSCT, especially the suppression of B lymphopoiesis resulting from GVHD, has been reported in clinical[4,27] and experimental[9,28-30] studies, we next investigated B lymphopoiesis in our GVHD model. To assess donor HSC–derived hematopoiesis, we used T cells from B6.SJL ($CD45.1^+$) mice and BM from (B6 × B6.SJL) F_1 ($CD45.1^+CD45.2^+$) mice in the [B6→BDF_1] transplantation model (Figure 2A). After day 14, more than 90% of BM cells were of $CD45.1^+CD45.2^+$ donor origin, and such complete donor chimerism was stable for all hematopoietic lineages examined until the end of our analysis on day 28 (data not shown). Flow cytometry showed that the numbers of $B220^+IgM^-$ B cells (B-cell precursors), $B220^+IgM^+$ B cells (immature and mature B cells), and $B220^+CD19^+c\text{-}Kit^+IgM^-$ cells (a class of pro-B cell) dramatically and continually fell in GVHD mice (Figure 2B-C), indicating the suppressed B lymphopoiesis. In contrast, T lymphopoiesis of donor BM origin gradually recovered even in the presence of GVHD (Figure 2D-E). Similar results were obtained for the spleen and peripheral blood (data not shown). Real-time reverse-transcription–polymerase chain reaction (RT-PCR) analysis of whole BM cells and sorted $Lin^-c\text{-}Kit^+$ BM cells on day 14 showed decreased expression of transcriptional factors essential for B lymphopoiesis,[31,32] that is E2A, early B-cell factor, and paired box gene 5, indicating that B lymphopoiesis was compromised at the earliest stages during GVHD (Figure 2F). Together with the suppression of lymphoid progenitors, these data indicate that B lymphopoiesis is compromised in its precursor level as well as lymphoid progenitor level.

Cellular mechanism for BM GVHD

Both $CD4^+$ and $CD8^+$ T cells are shown to induce GVHD in MHC-mismatched allo-HSCT.[33] To investigate the individual roles of $CD4^+$ and $CD8^+$ T cells in BM GVHD, we next analyzed the B lymphopoiesis in MHC class II– or class I–mismatched GVHD models. Purified $CD4^+$ or $CD8^+$ T cells, together with TCD BM from B6 donors, were infused into irradiated B6.C-$H2^{bm12}$ (bm12) or B6.C-$H2^{bm1}$ (bm1) recipients, respectively, and the numbers of B-cell precursors and immature and mature B cells in BM were evaluated on day 21 after allo-HSCT (Table 1). We found that bm12 recipient, and bm1 recipient to a lesser extent, developed severe impairment of B lymphopoiesis (supplemental Figure 2A). To further investigate the role of $CD4^+$ and $CD8^+$ T cells in BM GVHD, we also transferred graded numbers of $CD4^+$ T cells or $CD8^+$ T cells into BDF_1 (supplemental Figure 2B) or bm1/bm12 (similar results as BDF_1; data not shown) recipients. Again, we found that even a large number (2×10^7 cells) of $CD8^+$ T cells induced only moderate suppression of B lymphopoiesis, whereas the substantial suppression was induced by much smaller number (2×10^5 cells) of $CD4^+$ T cells (supplemental Figure 2B). These data suggest that donor $CD4^+$, and to a lesser extent $CD8^+$, T cells caused severe impairment of B lymphopoiesis in the MHC-mismatched GVHD models.

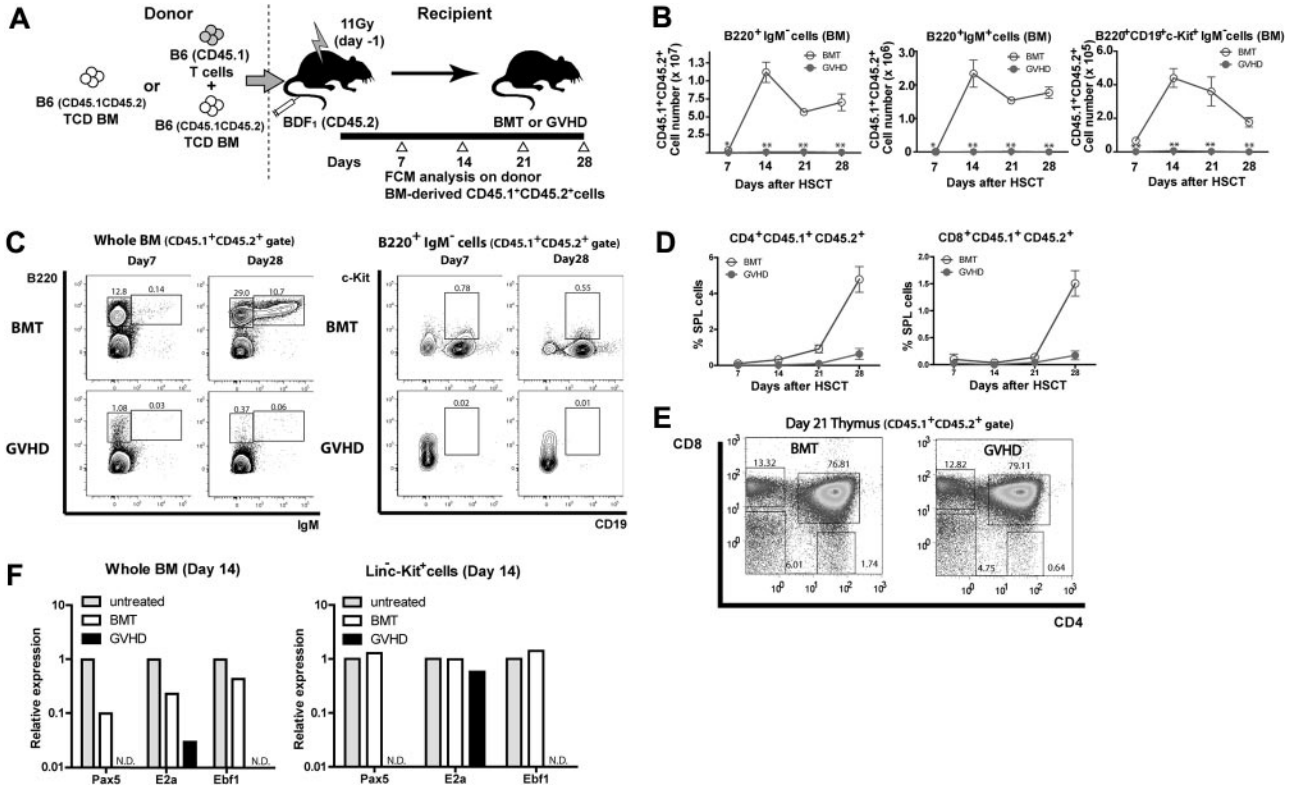

Figure 2. Suppression of B lymphopoiesis during GVHD. (A) Experimental scheme. TCD BM cells from (B6 × B6.SJL) F_1 (CD45.1$^+$CD45.2$^+$) mice with or without T cells from B6.SJL (CD45.1$^+$) mice were transplanted to lethally irradiated CD45.2$^+$ BDF_1 mice, and CD45.1$^+$CD45.2$^+$ donor BM–derived B and T lymphopoiesis was analyzed. (B-C) Flow cytometric analysis of B lymphopoiesis. (D) Donor BM-derived T lymphopoiesis. Kinetics of the frequency of CD4$^+$ and CD8$^+$ T cells in spleen. (E) Representative flow cytometric analysis of CD45.1$^+$CD45.2$^+$ thymic cells on day 21 after allo-HSCT. Cells were gated on CD45.1$^+$CD45.2$^+$ in each flow cytometric plot. Numbers in the plots represent the frequency of cells in adjacent gates. Data are representative of at least 3 independent experiments. Data are mean ± SE (n = 3 per group) in panels B and D. $^{**}P < .01$. (F) Real-time RT-PCR on day 14 after allo-HSCT in sorted Lin$^-$c-Kit$^+$ cells or whole BM. In each group, sorted cells from 5-8 mice were pooled and total RNA was isolated. Data are from one of 2 experiments with similar results. ND indicates not detectable.

We next evaluated the role of the Fas–Fas ligand (FasL) pathway in BM GVHD, as FasL-dependent donor T cell–mediated cytotoxicity has been implicated in the development of GVHD-associated lymphoid hypoplasia and B-cell immune dysfunction.[9] We transferred different combinations of purified T cells from FasL-defective B6$^{gld/gld}$ mice and BM from Fas-defective B6$^{lpr/lpr}$ mice into the [B6→BDF_1] transplantation model (Tables 1-2). Consistent with the previous report, recipients of FasL$^{gld/gld}$ T cells showed partial recovery of B lymphopoiesis (Figure 3A-B) and body weight (Figure 3C), whereas they were completely impaired in mice receiving wild-type (WT) B6-derived T cells. The recovery was not due to the defects in donor T-cell expansion, as we observed no differences in the numbers of T cells among GVHD groups (Figure 3D). Because Fas-FasL pathway–mediated cytotoxicity is independent of MHC class II–T-cell receptor interaction,[34,35] FasL$^+$CD4$^+$ T cells could directly impair both donor-derived hematopoietic cells and host-type radioresistant stroma that support hematopoiesis. To determine whether FasL$^+$CD4$^+$ T cells directly impair the donor-derived hematopoiesis via Fas-FasL pathway, we next used the B6$^{lpr/lpr}$ BM cells that are resistant to FasL mediated cytotoxicity. We found that B lymphopoiesis was completely impaired in mice received B6$^{lpr/lpr}$ BM and WT B6-derived T cells, demonstrating that BM GVHD is independent of the direct impairment of donor-derived hematopoietic cells by FasL$^+$ CD4$^+$ T cells. This result also suggests that host-type BM stroma could be a target of FasL$^+$ CD4$^+$ T cells. In addition, bm12 recipients of B6$^{gld/gld}$ CD4$^+$ T cells partially recovered B lymphopoiesis (supplemental Figure 2A), lymphoid progenitors, and thymic T-cell counts on day 28 (data not shown). These results indicated that FasL on donor CD4$^+$ T cells was partly responsible for the induction of BM GVHD.

Destruction of BM hematopoietic niches

The dispensable role of Fas expression on donor BM suggests that BM hematopoietic niches could be targets for GVHD, causing BM suppression and severe impairment of B lymphopoiesis. We directly tested this hypothesis using retransplantation experiments. First, to evaluate the damage to HSCs, lethally irradiated BDF_1 mice received TCD BM from either BMT or GVHD mice in the [B6→BDF_1] model ($^{[B6→BDF1]}$TCD BM→BDF_1). We found no significant differences in the numbers of B cells as well as monocytes and neutrophils between recipients of BMT- and GVHD-affected BM on day 14 after transplantation (Figure 4A). Second, to evaluate the damage to hematopoietic niches, TCD BM from normal B6.SJL donors was retransplanted into either BMT or GVHD recipient mice of the [B6→BDF_1] model on day 14, after 2 Gy TBI on day 13 (TCD BM→[B6→BDF_1]). We found that the numbers of B6.SJL donor-derived B cells profoundly, and also neutrophils and monocytes to a lesser extent, decreased in GVHD recipient mice on day 14 after retransplantation (Figure 4B). These results suggest that hematopoietic niche, but not HSCs, was affected by GVHD.

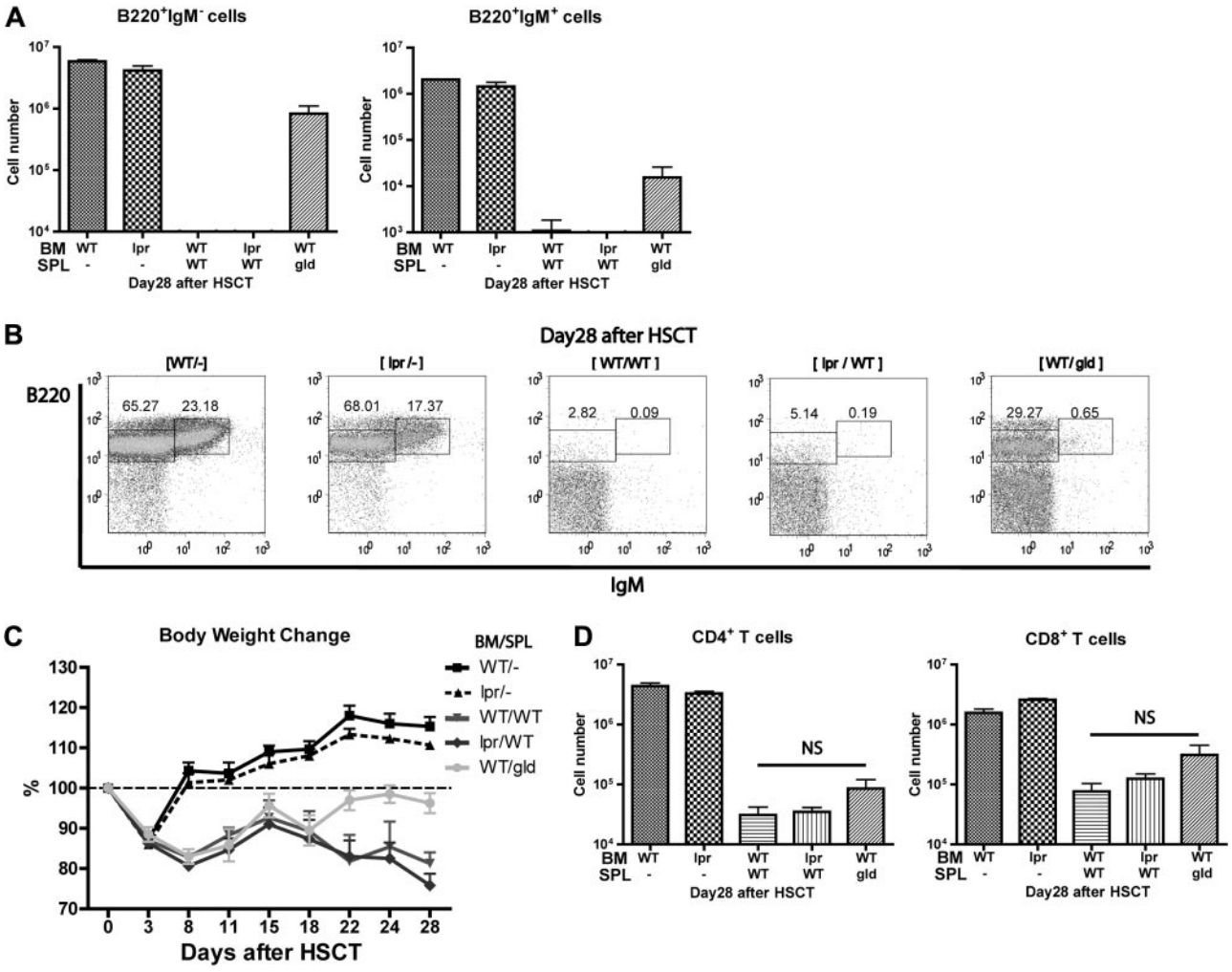

Figure 3. FasL$^+$ allogeneic CD4$^+$ T cells play a major role in BM GVHD. [B6→BDF$_1$] transplantation model using combinations of donor BM and spleen cells with different Fas or FasL genotype. In panel B, groups are labeled as source of BM/source of SPL on the flow cytometric representations and — indicates no splenic cells. Values represent mean and SE (n = 3-6). Experiments were performed at least twice. (A-B) Flow cytometric analysis of B220$^+$ and IgM$^+$ cells. (C) Body weight change. (D) Numbers of splenic CD4$^+$ and CD8$^+$ cells.

To further verify the competency of GVHD-affected HSCs, we performed long-term competitive repopulation analysis in syngeneic transplantation model using untreated BM as an internal control (Figure 4C). We found that BMT-derived BM reconstituted mature B and T cells more efficiently than GVHD-derived BM at 3 weeks after retransplantation. However, GVHD-affected BM reconstituted all hematopoietic cell subsets at 5 weeks, which was equal to or even higher than that of BMT-derived BM. These results indicate that GVHD-affected BM lack lymphoid-committed progenitors/precursors but retained sufficient number of functionally competent HSCs that could reconstitute hematopoiesis in an appropriate hematopoietic niche. Collectively, we supposed that recipient BM hematopoietic niches were destructed by donor T cells as the target of GVHD.

Osteoblastic niche as the target of GVHD in BM

To identify the target of GVHD within BM hematopoietic niche, we next performed the histologic analysis on bone sections from recipient mice with or without GVHD in the [B6→BDF$_1$] model. Time course analysis revealed that osteoblasts were completely lost from BM during GVHD as early as day 7 after allo-HSCT (Figure 5A). In addition, alkaline phosphatase (ALP; a marker of mature osteoblasts) reaction of fresh bone sections with ALP substrate revealed that ALP$^+$ osteoblasts on endosteal surface were completely lost in both cortical and trabecular bone of GVHD recipient mice by day 8 after allo-HSCT (Figure 5B). Furthermore, osteocalcin$^+$ cells almost completely disappeared in GVHD recipient mice by day 14 after allo-HSCT (supplemental Figure 3A). We also analyzed the functional defects of osteoblasts by evaluating bone formation using in vivo double fluorescent labeling with calcein on days 10 and 13 after allo-HSCT. Although 2 fluorescent lines, which reflect the newly formed bone layers, were observed in the trabecular bone of untreated and BMT recipient mice, we could not detect any calcein deposition in both trabecular and cortical bone of GVHD recipient mice (Figure 5C). As a result, parameters of bone formation and osteoblastic function, including osteoblast surface (ObS/BS [%]), osteoid surface (OS/BS [%]), mineralized surface (MS/BS [%]), mineral apposition rate (MAR [μm/d]), and bone formation rate (BFR/BS [$\mu m^3/\mu m^2/y$]) were not calculated, which indicated the impairment in the bone formation by osteoblasts during GVHD (Table 3). Furthermore, real-time RT-PCR analysis of whole tibia in each recipient mouse revealed that the markers of osteoblast differentiation, Runx2, Twist, Msx2, Osterix, Dlx5, and osteocalcin, significantly decreased in GVHD (Figure 5D). We concluded that

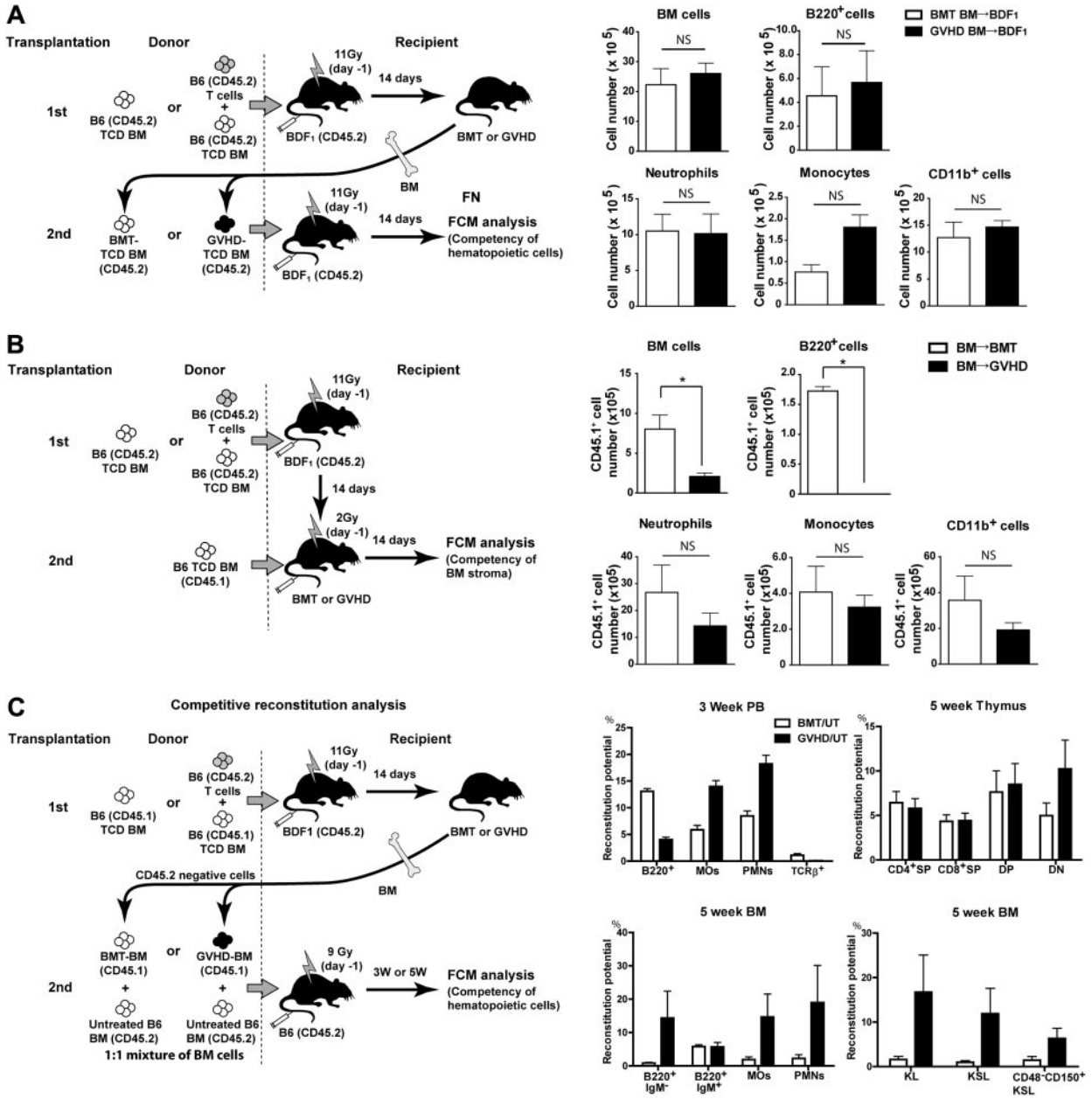

Figure 4. Impairment of BM hematopoietic niches during GVHD. (A-B) Reconstitution of leukocyte subsets at 2 weeks after retransplantation. (A) To evaluate the competency of hematopoietic cells, lethally irradiated BDF_1 mice received TCD BM from either BMT or GVHD recipient mice of the [B6→BDF_1] model ([B6→BDF1]TCD BM→BDF_1). (B) To evaluate the competency of BM stroma, TCD BM from normal C57BL/6.SJL donors was retransplanted into either BMT or GVHD recipient mice in the [B6→BDF_1] GVHD model on day 14, after TBI of 2 Gy on day 13 (TCD BM→[B6→BDF_1]). In the retransplantation, we performed nonmyeloablative irradiation (2 Gy) because recipient mice, especially GVHD mice, were susceptible to irradiation. We analyzed the donor BM–derived hematopoiesis based on the congenic marker CD45.1. Data are mean and SE (n = 3). *$P < .0001$. Experiments were performed at least twice. (C) In the long-term competitive repopulation analysis, we first transferred TCD BM cells from B6.SJL ($CD45.1^+$) with or without T cells from B6 ($CD45.2^+$) donor mice into $CD45.2^+$ BDF_1 recipient mice, generating BMT or GVHD group, respectively. On day 14 after transplantation, we killed these recipient mice and purified $CD45.1^+$ BM cells. We transferred 1:1 mixture of these $CD45.1^+$ BM cells from BMT or GVHD group and untreated normal TCD BM cells from B6 donor mice ($CD45.2^+$) into lethally irradiated B6 recipient mice ($CD45.2^+$). Graphs are the summary of flow cytometric analysis of hematopoietic recovery. Data are mean and SE (n = 3). MOs indicates monocytes; PMNs, polymorphonuclear leukocytes; KSL, c-$Kit^+Sca\text{-}1^+Lin^-$ cells; $CD4^+$SP, $CD4^+$ single-positive cells ($CD4^+CD8^-$); $CD8^+$SP, $CD8^+$ single-positive cells ($CD4^-CD8^+$); DP, double-positive cells ($CD4^+CD8^+$); DN, double-negative cells ($CD4^-CD8^-$); BMT/UT, the ratio of untreated B6-derived cells to BMT-derived cells (CD45.1/CD45.2); and GVHD/UT, the ratio of untreated B6-derived cells to GVHD-derived cells (CD45.1/CD45.2). Experiments were performed twice.

osteoblasts, a key component of hematopoietic niche,[12-15] are the target in BM GVHD.

We next examined the expression of MHC class II on osteoblasts to determine whether the loss of osteoblasts required direct recognition of osteoblasts by allo-$CD4^+$ T cells. Immunofluorescent staining revealed that osteoblasts did not express MHC class II in either BMT or GVHD recipient mice on day 3 when osteoblasts were still present even in GVHD group (supplemental Figure 3B), suggesting that the loss of osteoblasts does not require direct recognition of osteoblasts by allo-$CD4^+$ T cells.

Endothelial and CAR cell niches during GVHD

GVHD is a major risk factor for the many posttransplantation complications associated with vascular damage.[36-38] To further confirm vascular damage in GVHD-affected BM, we evaluated

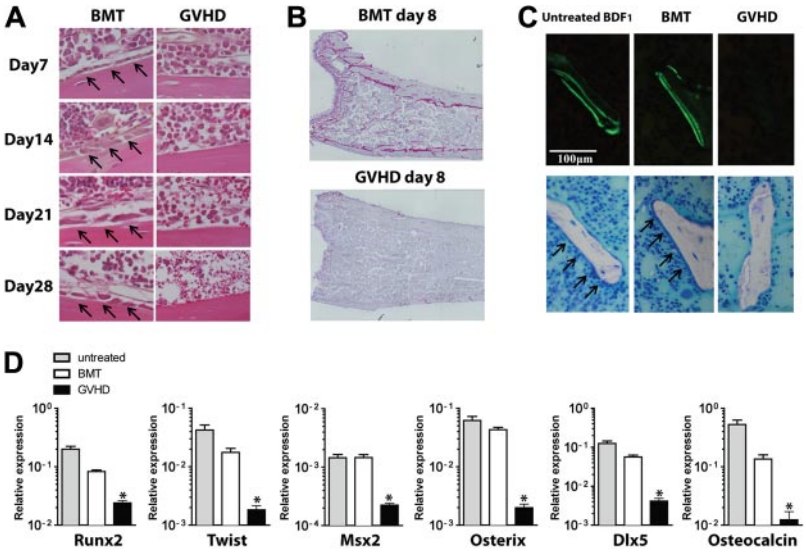

Figure 5. Destruction of osteoblastic niche during GVHD. (A-B) Histopathology of BM in [B6→BDF_1] transplantation model (n = 3 in each group; more than 5 sections per mouse were analyzed). (A) Arrows indicate osteoblasts (magnification ×400). (B) Staining for alkaline phosphatase (ALP) activity was performed on day 8 after allo-HSCT (magnification ×20). (C) Calcein double labeling and toluidine blue staining of tibiae in recipient mice ("Histopathologic analysis, immunofluorescence staining, and histomorphometric analysis"). Arrows indicate osteoblasts. (D) Real-time RT-PCR analysis of crushed whole tibia on day 14. Osteoblast differentiation markers Runx2, Twist, Msx2, Osterix, Dlx5, and osteocalcin were analyzed. Data are mean and SE (n = 4). Experiments were performed at least twice. *$P < .05$, vs untreated control group.

microvascular permeability using Evans blue (EB) dye extravasation assay.[39-42] We found significantly increased leakage of EB dye in the BM of GVHD mice (supplemental Figure 4A; $P < .05$), suggesting vascular damage caused by GVHD. Immunofluorescent staining of BM endothelial cells on day 14 after allo-HSCT revealed no remarkable differences between BMT and GVHD mice (supplemental Figure 4B). These results indicate the functional incompetence, but not the loss of endothelial cells, of the vasculature in the course of GVHD.

Together with osteoblasts, CAR cells play an important role in regulating HSCs and B lymphopoiesis in BM niches.[12,18,43] We next investigated damage to CAR cells during GVHD. Histologic analysis of GVHD BM from CXCL12–green fluorescent protein (GFP) knock-in BDF_1 recipients ($CXCL12^{GFP/+}$) showed that the number and morphology of CAR cells appeared to be unaffected on day 20 in the GVHD group (supplemental Figure 4C-D).

Treatment of BM GVHD

The histological analysis directly demonstrated the destruction of BM hematopoietic niches during early GVHD, which was primarily mediated by donor $CD4^+$ T cells, and also partially involved FasL. We next explored the effects of depleting $CD4^+$ T cells in vivo on the recovery of BM during GVHD. In the [B6→BDF_1] GVHD model, recipient mice were injected intraperitoneally with anti-CD4 and/or anti-CD8 mAb (200 μg each) on days 4 and 6 after allo-HSCT. Administering anti-CD4 mAb but not anti-CD8 mAb significantly improved B lymphopoiesis (supplemental Figure 5A-B), and simultaneously improved GVHD scores and body weight (supplemental Figure 5C). To ensure complete depletion of $CD8^+$ T cells, we also administered anti-CD8 mAb on days 4, 6, 14, and 21, and obtained similar results (data not shown). Anti-CD4 mAb treatment also ameliorated thymic damage (supplemental Figure 5D), and promoted naive $CD4^+$ and $CD8^+$ T-cell production from day 21 (supplemental Figure 5E). In addition, it also promoted the recovery of $Flt3^+IL\text{-}7R^+$ lymphoid progenitors and $CD48^-CD150^+KSL$ HSCs (supplemental Figure 5F). Azan staining and silver impregnation showed enhanced accumulation of elastic collagenous fibers preceding the recovery of osteoblasts in anti-CD4 mAb-treated GVHD mice, suggesting the process of stromal recovery after GVHD-induced damage (supplemental Figure 6). Taken together, our data suggest that the depletion of $CD4^+$ T cells early after allo-HSCT is an effective way for the prevention and the treatment of BM GVHD.

We also examined the recovery of humoral immunity, which is reportedly slow and is often further delayed in patients with GVHD.[4,5,44,45] Immunofluorescent staining revealed that IgA-producing cells were abolished in the small intestine of GVHD mice on day 14, whereas moderate number of IgA-producing cells was present in control BMT mice (supplemental Figure 7A). This observation paralleled the level of fecal IgA (supplemental Figure 7B). In GVHD mice treated with anti-CD4 mAb, serum Ig levels were almost undetectable on day 28 (data not shown); however, on day 100, both serum and fecal Ig levels had returned to normal in anti-CD4 mAb-treated mice (supplemental Figure 7C).

We next evaluated whether mAb treatment preserved graft-versus-tumor (GVT) activity. Recipient mice were injected intravenously with 1×10^4 P815 mastocytoma cells 2 hours before transplantation. All mice in the control BMT group died by day 18 as a result of dissemination of the P815 tumor, with symptoms such as liver masses and paralysis of the lower extremities (supplemental Figure 8A). The GVHD mice that received control purified rat IgG or anti-CD8 mAb died from GVHD with no evidence of P815 tumor cell dissemination at autopsy, suggesting that GVT effects had eliminated tumor cells (supplemental Figure 8B). Importantly,

Table 3. Histomorphometric analysis on day 14

	ObS/BS, %	OS/BS, %	MS/BS, %	MAR, μm/d	BFR/BS, $\mu m^3/\mu m^2/y$
Untreated BDF_1	17.3 ± 1.7	21.6 ± 2.8	25.7 ± 3.4	2.3 ± 0.3	24.7 ± 2.8
BMT	17.2 ± 6.5	15.3 ± 3.1	23.5 ± 7.5	1.5 ± 0.3	17.1 ± 6.6
GVHD	NC	NC	NC	NC	NC

Data are mean plus or minus SE (n = 4 per group).

ObS/BS indicates osteoblast surface per bone surface; OS/BS, osteoid surface per bone surface; MS/BS, mineralized surface per bone surface; MAR, mineral apposition rate; BFR/BS, bone formation rate per bone surface; and NC, not calculated.

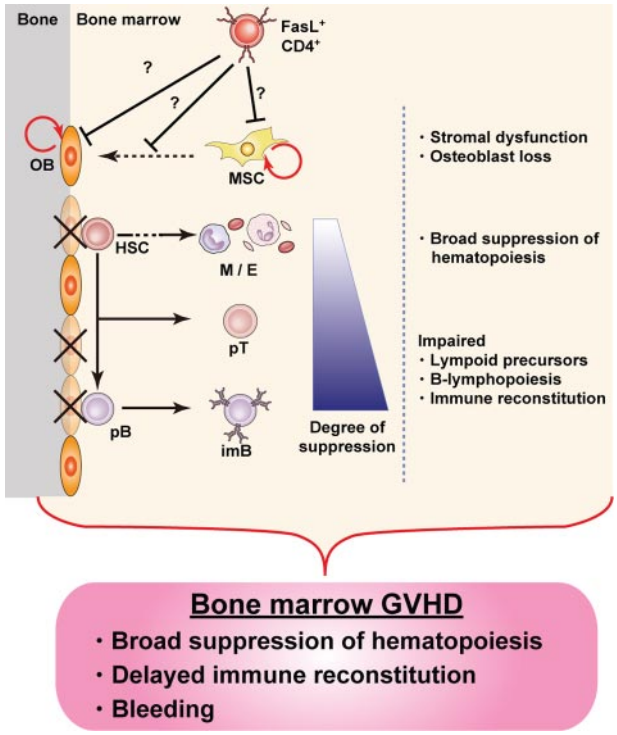

Figure 6. Concept of BM GVHD. BM appears to be a target for GVHD, with hematopoietic niches, especially those occupied by osteoblasts, being impaired soon after allo-HSCT. The damage is mediated by donor CD4$^+$ T cells, resulting in BM suppression, including B-lymphopoiesis disruption. The concept of BM GVHD provides an explanation for the symptoms associated with BM dysfunction, such as infections after delayed immune reconstitution. Depletion of CD4$^+$ T cells with anti-CD4 mAb could be a promising treatment to enhance BM recovery by minimizing GVHD while preserving the GVT effect. OB indicates osteoblast; HSC, hematopoietic stem cell; M, myeloid cells; E, erythroid cells; pT, T-cell precursor; pB, B-cell precursor; imB, immature B; and MSC, mesenchymal stem cell.

all GVHD mice treated with anti-CD4 mAb survived without symptoms of either GVHD or tumor progression. This showed that P815 tumor cells were eradicated by GVT effects, although anti-CD4 mAb alleviated the GVHD symptoms. These data suggest that anti-CD4 mAb treatment could preserve GVT activity while effectively preventing GVHD and promoting the recovery of humoral immune responses.

Discussion

Our results provide evidence for the destruction of BM hematopoietic niches during GVHD, resulting in BM suppression. We identified osteoblasts as a novel target for GVHD in the BM, the destruction of which occurred soon after allo-HSCT. Suppression of B lymphopoiesis during GVHD has been reported in both clinical and experimental studies,[4,9,27-30] and our current study unveils new details of the mechanisms involved in this phenomenon, focusing on the destruction of hematopoietic niches by donor T cells in the course of GVHD. Given the amassed evidence, here we propose the concept of "BM GVHD" (Figure 6).

The fact that GVHD-affected BM stroma failed to reconstitute the hematopoietic cells suggests the impairment of BM hematopoietic niche during GVHD. The BM microenvironment comprises multiple lineages, including fibroblast-like cells, adipocytes, osteoblasts, and endothelial cells. Recent studies have highlighted important roles for osteoblasts and the vasculature in maintaining HSC self-renewal and differentiation.[11,37,46-50] Results of BM staining for alkaline phosphatase (ALP) activity, histomorphometric analyses, and the expression of the markers of osteoblast differentiation clearly demonstrated the elimination of osteoblasts in the course of GVHD. Our observation that simultaneous impairment of osteoblasts and B lymphopoiesis occurs during GVHD is consistent with previous reports showing that ablation of osteogenic cells in vivo rapidly reduces the number of B cells preceding the loss of primitive hematopoietic precursors.[51,52] CAR cells also play a central role in regulating HSCs and B lymphopoiesis in BM niches.[12,18,43] Our model showed no drastic change in the number of CAR cells during GVHD. This discrepancy might be partly explained by functional impairment of CAR cells, which could play a pivotal role in B lymphopoiesis at different stages from other niche cells. After administering anti-CD4 mAb, B lymphopoiesis was restored before the complete recovery of osteoblasts (on day 28). This suggested an important role for CAR cells in supporting B lymphopoiesis after GVHD symptoms subsided. The osteoblast lineage is derived from putative mesenchymal stem cells, the origin of which, and relationships to other stromal cells (such as fibroblasts or CAR cells), remains unclear. Although the osteoblast lineage constitutes a niche for HSCs and supports differentiation of the B-lymphocyte lineage,[50] its interplay with perivascular cells, fibroblasts, and CAR cells in BM niches is largely unknown. In our GVHD model, direct damage to and impaired differentiation of osteoblasts are presumed to occur. However, our results did not rule out contributions from other BM stromal cell types to B lymphopoiesis, as many issues including the detailed molecular mechanisms should be addressed, given the differences in BM environment between GVHD and steady-state conditions.

Relative importance of allo-CD4$^+$ T cells led us to examine the expression of MHC class II on osteoblasts during GVHD. However, we did not detect the expression of MHC class II on osteoblasts in either BMT or GVHD on day 3 by immunofluorescent staining (supplemental Figure 3B). It is possible that MHC class II is required for the activation of alloantigen-specific CD4$^+$ T cells in the secondary lymphoid tissues, which then infiltrate into BM and mediate the destruction of osteoblasts via effector mechanism exerted independently of class II–T-cell receptor interaction. Meanwhile, recent literature has described populations of MHC class II$^+$ myeloid cells as an important cell type for the maintenance of osteoblastic niche. These cells, termed osteomacs[53,54] by several groups, could be the targets of GVHD and indirectly affect osteoblast integrity.

Our results using CD4$^+$ T cells from B6$^{gld/gld}$ mice supported the previous report that FasL on donor T cells was involved in impaired B lymphopoiesis during GVHD.[9] However, the MHC disparity in our fully mismatched model resulted in only partial involvement of the Fas-FasL pathway. During GVHD, inflammatory cytokines mediate target destruction and consequent mortality, particularly in CD4-mediated GVHD and at least partly in CD8-mediated GVHD.[55] We compared the levels of major cytokines in supernatants from BM culture for 24 hours and uncultured, freshly flushed BM between the BMT and GVHD groups, and found no significant differences in those thought to be involved in GVHD, such as IL-1, tumor necrosis factor-α, and interferon-γ (data not shown). Furthermore, tumor necrosis factor-α and interferon-γ deficiencies in donor T cells did not restore B lymphopoiesis in our model (data not shown). This suggests that inflammatory cytokines may be dispensable for BM GVHD mediated by CD4$^+$ T cells. Precise understanding of how donor T cells recognize and destruct host

BM stroma will lead to the clarification of the detailed mechanism for BM GVHD.

Early treatment with anti-CD4 mAbs, on days 4 and 6 after allo-HSCT, ameliorated BM GVHD and prolonged survival while maintaining GVT effects. In contrast, treatment with anti-CD4 mAb on days 14 and 16 failed to restore BM function (data not shown), suggesting that damage to hematopoietic niche occurred soon after allo-HSCT. Consistent with these findings, we found that destruction of osteoblasts is completed as early as day 7 with the accumulation of effector $CD4^+$ T cells in BM, which is much earlier than the manifestation of systemic GVHD. In addition, B lymphopoiesis is also inhibited in GVHD mice from day 7 (Figure 2B-C). Together, these data indicate that BM GVHD is not secondary to severe systemic GVHD, but is independently completed before the development of severe systemic GVHD. Our results suggest that anti-CD4 mAb could be a promising therapy to prevent GVHD in allo-HSCT. However, these findings must be cautiously evaluated before they can be generalized and applied to outbred, large animals and human patients, in whom allo-HSCT is usually performed using MHC-identical donors.

In conclusion, we identified BM as a novel target for GVHD, which was manifested by $CD4^+$ T cell–mediated impairment of hematopoietic niches supported by osteoblasts soon after allo-HSCT. The concept of BM GVHD (Figure 6) would provide an explanation for disrupted hematopoiesis and delayed immune reconstitution in the clinical settings, given that no comprehensive analysis has been reported so far. Our findings will provide a clue to the understanding of cellular and molecular mechanism for BM suppression in GVHD and the development of a novel therapy enabling the BM recovery by minimizing GVHD while preserving the GVT effect.

Acknowledgments

We thank S. Hashimoto and S. Ishikawa for helpful discussions and suggestions; A. Hoshino and T. Dohi for technical support with the cytokine analysis and equipment; S. Aoki, Y. Morishita, and K. Sakuma for assistance with immunohistology; S. Fujita, Y. Harukawa, J. Kurachi, Y. Lee, K. Ogoshi, M. Ogawa, Y. Hosono, S. Iwashita, and Y. Arakawa for assistance; and the Center for NanoBio Integration of The University of Tokyo for the use of BD LSR II flow cytometer.

Authorship

Contribution: Y.S. and S.U. formulated the basic hypotheses and designed experiments; Y.S. performed most of the experiments, analyzed data, and wrote the paper with assistance from S.U., J.A., Y.W., and M.K.; S.U. designed and performed experiments, analyzed data, and supervised the study; T.S. and T.N. designed and performed the CAR cell analysis; Y.M. performed the pathologic analysis; M.I. analyzed data and supervised the study; K.M. designed experiments, analyzed data, and supervised the study; and all authors discussed the results and commented on the paper.

Conflict-of-interest disclosure: The authors declare no competing financial interests.

Correspondence: Kouji Matsushima, Department of Molecular Preventive Medicine, Graduate School of Medicine, The University of Tokyo, 7-3-1, Hongo, Bunkyo-ku, Tokyo, 113-0033, Japan; e-mail: koujim@m.u-tokyo.ac.jp.

References

1. Glucksberg H, Storb R, Fefer A, et al. Clinical manifestations of graft-versus-host disease in human recipients of marrow from HL-A-matched sibling donors. *Transplantation.* 1974;18(4):295-304.
2. Yanik G, Cooke KR. The lung as a target organ of graft-versus-host disease. *Semin Hematol.* 2006; 43(1):42-52.
3. The Japan Society for Hematopoietic Cell Transplantation Office of Nationwide Survey. Annual Report of Nationwide Survey 2003. Nagoya, Japan: Nagoya University Daiko Medical Center.
4. Abrahamsen IW, Somme S, Heldal D, Egeland T, Kvale D, Tjonnfjord GE. Immune reconstitution after allogeneic stem cell transplantation: the impact of stem cell source and graft-versus-host disease. *Haematologica.* 2005;90(1):86-93.
5. Peggs KS. Immune reconstitution following stem cell transplantation. *Leuk Lymphoma.* 2004;45(6): 1093-1101.
6. Crooks GM, Weinberg K, Mackall C. Immune reconstitution: from stem cells to lymphocytes. *Biol Blood Marrow Transplant.* 2006;12(1 suppl 1):42-46.
7. Imamura M. Immunological reconstitution and immunoregulatory cells in hematopoietic stem cell transplantation. *Int J Hematol.* 2002;76(suppl 1):191-194.
8. Iwasaki T, Hamano T, Saheki K, et al. Effect of graft-versus-host disease (GVHD) on host hematopoietic progenitor cells is mediated by Fas-Fas ligand interactions but this does not explain the effect of GVHD on donor cells. *Cell Immunol.* 1999;197(1):30-38.
9. Baker MB, Riley RL, Podack ER, Levy RB. Graft-versus-host-disease-associated lymphoid hypoplasia and B cell dysfunction is dependent upon donor T cell-mediated Fas-ligand function, but not perforin function. *Proc Natl Acad Sci U S A.* 1997; 94(4):1366-1371.
10. Mori T, Nishimura T, Ikeda Y, Hotta T, Yagita H, Ando K. Involvement of Fas-mediated apoptosis in the hematopoietic progenitor cells of graft-versus-host reaction-associated myelosuppression. *Blood.* 1998;92(1):101-107.
11. Wilson A, Trumpp A. Bone-marrow haematopoietic-stem-cell niches. *Nat Rev Immunol.* 2006; 6(2):93-106.
12. Arai F, Hirao A, Ohmura M, et al. Tie2/angiopoietin-1 signaling regulates hematopoietic stem cell quiescence in the bone marrow niche. *Cell.* 2004; 118(2):149-161.
13. Calvi LM, Adams GB, Weibrecht KW, et al. Osteoblastic cells regulate the haematopoietic stem cell niche. *Nature.* 2003;425(6960):841-846.
14. Zhang J, Niu C, Ye L, et al. Identification of the haematopoietic stem cell niche and control of the niche size. *Nature.* 2003;425(6960):836-841.
15. Kiel MJ, Yilmaz OH, Iwashita T, Terhorst C, Morrison SJ. SLAM family receptors distinguish hematopoietic stem and progenitor cells and reveal endothelial niches for stem cells. *Cell.* 2005; 121(7):1109-1121.
16. Egawa T, Kawabata K, Kawamoto H, et al. The earliest stages of B cell development require a chemokine stromal cell-derived factor/pre-B cell growth-stimulating factor. *Immunity.* 2001;15(2): 323-334.
17. Nagasawa T, Hirota S, Tachibana K, et al. Defects of B-cell lymphopoiesis and bone-marrow myelopoiesis in mice lacking the CXC chemokine PBSF/SDF-1. *Nature.* 1996;382(6592):635-638.
18. Sugiyama T, Kohara H, Noda M, Nagasawa T. Maintenance of the hematopoietic stem cell pool by CXCL12-CXCR4 chemokine signaling in bone marrow stromal cell niches. *Immunity.* 2006;25(6):977-988.
19. Tokoyoda K, Egawa T, Sugiyama T, Choi BI, Nagasawa T. Cellular niches controlling B lymphocyte behavior within bone marrow during development. *Immunity.* 2004;20(6):707-718.
20. Ara T, Tokoyoda K, Sugiyama T, Egawa T, Kawabata K, Nagasawa T. Long-term hematopoietic stem cells require stromal cell-derived factor-1 for colonizing bone marrow during ontogeny. *Immunity.* 2003;19(2):257-267.
21. Cooke KR, Kobzik L, Martin TR, et al. An experimental model of idiopathic pneumonia syndrome after bone marrow transplantation: I, the roles of minor H antigens and endotoxin. *Blood.* 1996; 88(8):3230-3239.
22. Ueha S, Murai M, Yoneyama H, et al. Intervention of MAdCAM-1 or fractalkine alleviates graft-versus-host reaction associated intestinal injury while preserving graft-versus-tumor effects. *J Leukoc Biol.* 2007;81(1):176-185.
23. Akadegawa K, Ishikawa S, Sato T, et al. Breakdown of mucosal immunity in the gut and resultant systemic sensitization by oral antigens in a murine model for systemic lupus erythematosus. *J Immunol.* 2005;174(9):5499-5506.
24. Karsunky H, Inlay MA, Serwold T, Bhattacharya D, Weissman IL. Flk2+ common lymphoid progenitors possess equivalent differentiation potential for the B and T lineages. *Blood.* 2008;111(12): 5562-5570.
25. Akashi K, Traver D, Miyamoto T, Weissman IL. A clonogenic common myeloid progenitor that gives rise to all myeloid lineages. *Nature.* 2000;404(6774):193-197.
26. Socolovsky M, Nam H, Fleming MD, Haase VH,

Brugnara C, Lodish HF. Ineffective erythropoiesis in Stat5a(-/-)5b(-/-) mice due to decreased survival of early erythroblasts. *Blood.* 2001;98(12):3261-3273.

27. Storek J, Wells D, Dawson MA, Storer B, Maloney DG. Factors influencing B lymphopoiesis after allogeneic hematopoietic cell transplantation. *Blood.* 2001;98(2):489-491.
28. Xenocostas A, Osmond DG, Lapp WS. The effect of the graft-versus-host reaction on B lymphocyte production in bone marrow of mice: depressed genesis of early progenitors prior to mu heavy chain expression. *Transplantation.* 1991;51(5):1089-1096.
29. Garvy BA, Elia JM, Hamilton BL, Riley RL. Suppression of B-cell development as a result of selective expansion of donor T cells during the minor H antigen graft-versus-host reaction. *Blood.* 1993;82(9):2758-2766.
30. Falzarano G, Krenger W, Snyder KM, Delmonte J Jr, Karandikar M, Ferrara JL. Suppression of B-cell proliferation to lipopolysaccharide is mediated through induction of the nitric oxide pathway by tumor necrosis factor-alpha in mice with acute graft-versus-host disease. *Blood.* 1996;87(7):2853-2860.
31. Busslinger M. Transcriptional control of early B cell development. *Annu Rev Immunol.* 2004;22:55-79.
32. Hardy RR, Hayakawa K. B cell development pathways. *Annu Rev Immunol.* 2001;19:595-621.
33. Shlomchik WD. Graft-versus-host disease. *Nat Rev Immunol.* 2007;7(5):340-352.
34. Stalder T, Hahn S, Erb P. Fas antigen is the major target molecule for CD4+ T cell-mediated cytotoxicity. *J Immunol.* 1994;152(3):1127-1133.
35. Erb P, Grogg D, Troxler M, Kennedy M, Fluri M. CD4+ T cell-mediated killing of MHC class II-positive antigen-presenting cells, I: characterization of target cell recognition by in vivo or in vitro activated CD4+ killer T cells. *J Immunol.* 1990;144(3):790-795.
36. Hale GA, Bowman LC, Rochester RJ, et al. Hemolytic uremic syndrome after bone marrow transplantation: clinical characteristics and outcome in children. *Biol Blood Marrow Transplant.* 2005;11(11):912-920.
37. Richardson P, Guinan E. Hepatic veno-occlusive disease following hematopoietic stem cell transplantation. *Acta Haematol.* 2001;106(1-2):57-68.
38. Nürnberger W, Willers R, Burdach S, Gobel U. Risk factors for capillary leakage syndrome after bone marrow transplantation. *Ann Hematol.* 1997;74(5):221-224.
39. Reutershan J, Cagnina RE, Chang D, Linden J, Ley K. Therapeutic anti-inflammatory effects of myeloid cell adenosine receptor A2a stimulation in lipopolysaccharide-induced lung injury. *J Immunol.* 2007;179(2):1254-1263.
40. Miller DL, Quddus J. Diagnostic ultrasound activation of contrast agent gas bodies induces capillary rupture in mice. *Proc Natl Acad Sci U S A.* 2000;97(18):10179-10184.
41. Lin MI, Yu J, Murata T, Sessa WC. Caveolin-1-deficient mice have increased tumor microvascular permeability, angiogenesis, and growth. *Cancer Res.* 2007;67(6):2849-2856.
42. Kamath AF, Chauhan AK, Kisucka J, et al. Elevated levels of homocysteine compromise blood-brain barrier integrity in mice. *Blood.* 2006;107(2):591-593.
43. Nagasawa T. Microenvironmental niches in the bone marrow required for B-cell development. *Nat Rev Immunol.* 2006;6(2):107-116.
44. Novitzky N, Davison GM. Immune reconstitution following hematopoietic stem-cell transplantation. *Cytotherapy.* 2001;3(3):211-220.
45. André-Schmutz I, Dal Cortivo L, Fischer A, Cavazzana-Calvo M. Improving immune reconstitution while preventing GvHD in allogeneic stem cell transplantation. *Cytotherapy.* 2005;7(2):102-108.
46. Sacchetti B, Funari A, Michienzi S, et al. Self-renewing osteoprogenitors in bone marrow sinusoids can organize a hematopoietic microenvironment. *Cell.* 2007;131(2):324-336.
47. Adams GB, Scadden DT. The hematopoietic stem cell in its place. *Nat Immunol.* 2006;7(4):333-337.
48. Lo Celso C, Fleming HE, Wu JW, et al. Live-animal tracking of individual haematopoietic stem/progenitor cells in their niche. *Nature.* 2009;457(7225):92-96.
49. Xie Y, Yin T, Wiegraebe W, et al. Detection of functional haematopoietic stem cell niche using real-time imaging. *Nature.* 2009;457(7225):97-101.
50. Wu JY, Scadden DT, Kronenberg HM. Role of the osteoblast lineage in the bone marrow hematopoietic niches. *J Bone Miner Res.* 2009;24(5):759-764.
51. Visnjic D, Kalajzic Z, Rowe DW, Katavic V, Lorenzo J, Aguila HL. Hematopoiesis is severely altered in mice with an induced osteoblast deficiency. *Blood.* 2004;103(9):3258-3264.
52. Zhu J, Garrett R, Jung Y, et al. Osteoblasts support B-lymphocyte commitment and differentiation from hematopoietic stem cells. *Blood.* 2007;109(9):3706-3712.
53. Pettit AR, Chang MK, Hume DA, Raggatt LJ. Osteal macrophages: a new twist on coupling during bone dynamics. *Bone.* 2008;43(6):976-982.
54. Chang MK, Raggatt LJ, Alexander KA, et al. Osteal tissue macrophages are intercalated throughout human and mouse bone lining tissues and regulate osteoblast function in vitro and in vivo. *J Immunol.* 2008;181(2):1232-1244.
55. Teshima T, Ordemann R, Reddy P, et al. Acute graft-versus-host disease does not require alloantigen expression on host epithelium. *Nat Med.* 2002;8(6):575-581.